

DRAFT μ FLU08-162

FLUID PROPULSION IN MICROCHANNELS USING MAGNETICALLY ACTUATED ARTIFICIAL CILIA - A PARAMETRIC STUDY

Syed, Khaderi

Zernike Institute for Advanced Materials, University of Groningen, Nijenborgh 4, 9747AG Groningen,
The Netherlands
s.n.khaderi@rug.nl

Michiel, Baltussen, Patrick, Anderson

Technische Universiteit Eindhoven, Den Dolech 1, 5600 MB Eindhoven, The Netherlands
m.g.h.m.baltussen@tue.nl, p.d.anderson@tue.nl

Daniel, Ioan

Politehnica University of Bucharest, Spl. Independentei 313, 77206 Bucharest, Romania
daniel@lmn.pub.ro

Jaap, den Toonder

Philips Research, High Tech Campus 4, 5656 AZ Eindhoven, The Netherlands
jaap.den.toonder@philips.com

Patrick, Onck¹

Zernike Institute for Advanced Materials, University of Groningen, Nijenborgh 4, 9747AG Groningen,
The Netherlands
p.r.onck@rug.nl

KEY WORDS

Microfluidic actuators, Artificial cilia, Low Reynolds number fluid flow, Magnetic thin film

ABSTRACT

In this work we propose magnetic actuators, which are actuated by an external field, to propel fluids in micro channels of microTAS applications. The proposed actuators are thin polymer films with embedded magnetic nano particles. As the fluid propulsion takes place at low Reynolds number at these length scales, the actuator should move in an asymmetric manner. By tuning the film geometry, magnetic nature of the particles and the applied field, we are able to design actuators which are able to move in an asymmetric manner. With the help of coupled computational fluid dynamic (CFD) simulations, we prove that this asymmetric motion indeed leads to a net fluid flow. We identify the dimensionless parameters governing the motion of the actuators and we characterize their behavior in terms of these parameters.

¹ Corresponding author

1. INTRODUCTION

One of the sectors of bio-technology with an intense current research activity is the development of lab-on-a-chip devices to analyse bio-fluids. A typical lab-on-a-chip consists of a network of micro-channels and micro-chambers, in which the fluid must be manipulated, and operations like fluid propulsion, mixing [1, 2], separation and detection of bio-molecules must take place. The fluid flow in micro-channels for these applications occurs at low Reynolds number. If the fluid to be analyzed has to be propelled by an actuator, then the actuator should move in a cyclic but asymmetric manner. Such an asymmetric motion occurs in biological hair-like structures called cilia (for example, in the human respiratory system, or on the outer surface of micro-organisms), which propel the fluid around them. Recently, attempts have been made to synthesize micro actuators based on this principle for mixing [1] and transportation [3]. In this work we design and quantify actuators which can mimic the motion of a biological cilium. These actuators, or artificial cilia, are thin compliant films in which magnetic particles are dispersed, and that can be actuated by an external magnetic field. Depending on the nature of the particles, the film can be either permanently magnetic (PM) or super-paramagnetic (SPM). The thin film is modeled using 2D finite elements, taking inertia and geometric nonlinearity into account. For the parametric study, the fluid is assumed to exert a velocity-proportional drag force on the film. The specific values of the drag coefficients used in the simulations have been calibrated through a comparison with a coupled solid-fluid model. The coupled solid-fluid calculations show that fluid is propelled in proportion to the area swept by the actuator tip. We have identified three distinct mechanisms in which the actuator can move in an asymmetric manner by manipulating the external magnetic field in time. Three dimensionless numbers are identified which govern the behavior of the actuator system. These are the magneto-elastic number (the ratio of magnetic to elastic force), the inertia number (the ratio of inertia to elastic force) and the fluid number (the ratio of viscous to elastic force). The actuator system is fully described by these three nondimensional parameters. As a measure of the effectiveness of fluid propulsion, we use the area swept by the free end of the film and the time taken by the film to complete one cycle. The effectiveness of the actuator system is finally quantified as a function of the three dimensionless parameters.

2. MAGNETO-MECHANICAL MODEL

2.1 Equations of motion

As a starting point for the Euler-Bernoulli beam element formulation we use the principle of virtual work [4]. In the weak form of the equations of motion, the virtual work of the external forces is equal to the internal work and is given by

$$\delta W_{\text{int}}^t = \delta W_{\text{ext}}^t, \quad (1)$$

with

$$\delta W_{\text{int}}^t = \int (\sigma \delta \varepsilon + \rho (\ddot{u} \delta u + \ddot{v} \delta v)) dV, \quad (2)$$

where δ is the variational operator, u and v are the axial and transverse displacements along the beam length (axial coordinate x) and ρ is the density of the film. Furthermore, σ is the axial stress and ε is the corresponding strain, given by

$$\varepsilon = \partial u / \partial x + (\partial v / \partial x)^2 / 2 - y \partial^2 v / \partial x^2 \equiv \bar{\varepsilon} - y \chi.$$

By substituting the strains and defining $\int \sigma dA = P$ and $-\int \sigma y dA = M$ (A is the area of the cross section), the internal virtual work at time t can be written as the sum of an elastic and an inertial part. Subsequently, the internal virtual work at time $t + \Delta t$ is written as

$$\delta W_{\text{int}}^{t+\Delta t} = \int (P^{t+\Delta t} \delta \bar{\varepsilon}^{t+\Delta t} + M^{t+\Delta t} \delta \chi^{t+\Delta t} + \rho A (\dot{u}^{t+\Delta t} \delta u + \dot{v}^{t+\Delta t} \delta v)) dx. \quad (3)$$

The corresponding external virtual work is

$$\delta W_{\text{ext}}^{t+\Delta t} = \int \left(f_x^{t+\Delta t} \delta u + f_y^{t+\Delta t} \delta v + N_z^{t+\Delta t} \frac{\partial \delta v}{\partial x} \right) A dx + \int (t_x^{t+\Delta t} \delta u + t_y^{t+\Delta t} \delta v) b dx \quad (4)$$

where f_x and f_y are the magnetic body forces in axial and transverse directions, N_z is the magnetic body couple in the out-of-plane direction, t_x and t_y are the surface tractions due to the fluid drag and b is the out-

of-plane thickness of the film. The axial and transverse displacements are linearly and cubically interpolated in terms of the nodal degrees of freedom, the displacements and rotations, $u = N_u \mathbf{p}$, $v = N_v \mathbf{p}$ where $\mathbf{p} = [u_1 \ v_1 \ \phi_1 l_0 \ u_2 \ v_2 \ \phi_2 l_0]^T$, N_u and N_v being the standard interpolation matrices. We now expand the elastic part of internal virtual work linearly in time. Neglecting higher order terms, by using the following notation $\partial u / \partial x = \mathbf{B}_u \mathbf{p}$, $\partial v / \partial x = \mathbf{B}_v \mathbf{p}$, $\partial^2 u / \partial x^2 = \mathbf{C}_v \mathbf{p}$, the constitutive relations $\Delta P = EA \Delta \bar{\epsilon}$, $\Delta M = EI \Delta \chi$ with E being the elastic modulus, I being the second moment of area defined as $I = bh^3 / 12$ (h being the thickness of the film), and choosing the domain of integration to be the current configuration, the total displacements are zero, $\mathbf{p} = 0$, we get

$$\delta W_{\text{int}}^{t+\Delta t} = \delta \mathbf{p}^T \mathbf{f}_{\text{int}} + \delta \mathbf{p}^T \mathbf{K} \Delta \mathbf{p} + \delta \mathbf{p}^T \mathbf{M} \dot{\mathbf{p}}^{t+\Delta t}, \quad (5)$$

where

$$\mathbf{f}_{\text{int}} = \int \left[P^T \mathbf{B}_u^T + M^T \mathbf{C}_v^T \right] dx$$

is the nodal internal force vector, and

$$\mathbf{K} = \int \left[EAB_u^T \mathbf{B}_u + EIC_v^T \mathbf{C}_v + P^t \mathbf{B}_v^T \mathbf{B}_v \right] dx$$

is the stiffness matrix. The first two terms of which represent the material stiffness and the third term represents the geometric stiffness, and \mathbf{M} in Eqn. 5 is the consistent mass matrix. The external virtual work is

$$\delta W_{\text{int}}^{t+\Delta t} = \delta \mathbf{p}^T \int \left[\left(f_x^{t+\Delta t} \mathbf{N}_u^T + f_y^{t+\Delta t} \mathbf{N}_v^T + N_z^{t+\Delta t} \mathbf{B}_v^T \right) A + b \left(t_x^{t+\Delta t} \mathbf{N}_u^T + t_y^{t+\Delta t} \mathbf{N}_v^T \right) \right] = \delta \mathbf{p}^T \mathbf{f}_{\text{ext}}^{t+\Delta t}. \quad (6)$$

By equating the internal and external virtual work and noting that the resulting equation holds for arbitrary $\delta \mathbf{p}$ we get

$$\mathbf{K} \Delta \mathbf{p} + \mathbf{M} \dot{\mathbf{p}} = \mathbf{f}_{\text{ext}}^{t+\Delta t} - \mathbf{f}_{\text{int}}^t. \quad (7)$$

The motion of the film with time is obtained by solving Eqn. 7 with appropriate initial and boundary conditions. Equation 7 is integrated in time using Newmark's method to solve for the nodal accelerations, which are then integrated to get the nodal displacements and velocities. The drag forces of the fluid on the film are accounted for through the surface tractions in Eqn. 6. The tractions are proportional to the velocity in the low Reynolds number regime, with the normal and tangential coefficients of proportionality (the drag coefficients) denoted by C_x and C_y . The tractions are calculated from the velocity at time t . The magnetic forces come in through the body forces and couples in Eqn. 6. These are calculated by solving Maxwell's equations on the current configuration, i.e. the configuration at time t (see section 2.2).

2.2 Magnetostatics

Maxwell's equations for the magnetostatic problem with no currents are

$$\nabla \cdot \mathbf{B} = 0, \quad \nabla \times \mathbf{H} = 0, \quad (8)$$

with the constitutive relation $\mathbf{B} = \mu_0 (\mathbf{M} + \mathbf{H})$, where \mathbf{B} is the magnetic flux density, \mathbf{H} is the magnetic field, \mathbf{M} is the magnetization which includes the remanent magnetization, and μ_0 is the permeability of vacuum. The general solution of the Eqn. 8 can be found [5], resulting in a Green's function, which contains a volumetric term and a surface term. We now discretize the film into a chain of rectangular segments. \mathbf{M} is uniform inside the segment and zero outside the segment. On the surface of each segment there is a jump of magnetization. The magnetic field in local coordinates (denoted by $\hat{\cdot}$) due to the four surfaces of a segment can now be calculated at any position (\hat{x}, \hat{y}) by evaluating the surface integral in the above mentioned Green's function. This results in an equation of the form $\hat{\mathbf{H}}_i = \mathbf{G}_i \hat{\mathbf{M}}_i$, where $\hat{\mathbf{M}} = [\hat{M}_x \ \hat{M}_y]^T$, $\hat{\mathbf{H}} = [\hat{H}_x \ \hat{H}_y]^T$ and \mathbf{G}_i contains the geometric information about the segment and the point under consideration. The field due to segment i with respect to the global coordinates is $\mathbf{H}_i = \mathbf{R}_i \hat{\mathbf{H}}_i$, where \mathbf{R}_i is the transformation matrix. The field at any element j because of the magnetization of all the segments throughout the film, in local coordinates, is

$$\hat{\mathbf{H}}_j = \mathbf{R}_j^T \mathbf{H}_0 + \sum_{i=1}^N \mathbf{R}_j^T \mathbf{R}_i \mathbf{G}_{ij} \hat{\mathbf{M}}_i, \quad (9)$$

where \mathbf{H}_0 is the externally applied magnetic field and N is the total number of segments. For the situation of a permanently magnetized film with magnetization $\hat{\mathbf{M}}_i$, $i=1, \dots, N$, Eqn. 9 gives the magnetic field in all the segments. However, in case of a super-paramagnetic film, the magnetization $\hat{\mathbf{M}}$ is not known a-priori, but depends on the local magnetic field through

$$\hat{\mathbf{M}}_j = \hat{\chi} \hat{\mathbf{H}}_j = \hat{\chi} \mathbf{R}_j^T \mathbf{H}_0 + \sum_{i=1}^N \hat{\chi} \mathbf{R}_j^T \mathbf{R}_i \mathbf{G}_{ij} \hat{\mathbf{M}}_i,$$

with $\hat{\chi}$ the susceptibility tensor. There are N similar pairs of equations. In total these are $2 \times N$ equations for the $2 \times N$ unknown magnetizations. This set of equations is solved to get the magnetization. Once the magnetization is known the field can be found from Eqn. 9. Then the magnetic flux density can be found by using the constitutive relation.

3. DIMENSIONAL ANALYSIS

To identify the dimensionless parameters that govern the behavior of the system, we start from the virtual work equation (see section 2.1), neglecting the axial deformations:

$$\int EI \frac{\partial^2 v}{\partial x^2} \frac{\partial^2 \delta v}{\partial x^2} dx + \int \rho A \frac{\partial^2 v}{\partial t^2} \delta v dx = \int N_z \frac{\partial \delta v}{\partial x} A dx - \int C_y \frac{\partial v}{\partial t} b \delta v dx,$$

where the first term represents the virtual elastic work done by the internal moments, the second term represents the virtual work done by the inertial forces, the third term represents the virtual work done by the magnetic couple and the last term represents the work done by the fluid drag forces. This is valid for any segment dx , and hence the force terms can be written in local form. We introduce the dimensionless variables V , T and X , such that $v = VL$, $x = XL$ and $t = T t_{\text{ref}}$, where L is a characteristic length (taken to be the length of the film) and t_{ref} is a characteristic time. Substitution yields

$$\frac{Ebh^3}{12L^2} \frac{\partial^2 V}{\partial X^2} \frac{\partial^2 \delta V}{\partial X^2} + \frac{\rho bhL^2}{t_{\text{ref}}^2} \delta V \frac{\partial^2 V}{\partial T^2} = N_z hb \frac{\partial \delta V}{\partial X} - \frac{C_y L^2 b}{t_{\text{ref}}} \frac{\partial V}{\partial T} \delta V,$$

from which the elastic $Ebh^3/12L^2$, the inertial $\rho bhL^2/t_{\text{ref}}^2$, the viscous $C_y L^2 b/t_{\text{ref}}$ and the magnetic ($N_z hb$) terms can be identified. By normalising with the elastic term we get the three governing dimensionless numbers: Inertia number $I_n = 12\rho L^4 / Eh^2 t_{\text{ref}}^2$ the ratio of inertial to elastic force, magneto-elastic number $M_n = 12N_z L^2 / Eh^2$ the ratio of magnetic to elastic force and fluid number $F_n = 12C_y L^4 / Eh^3 t_{\text{ref}}$ the ratio of fluid to elastic force. Before proceeding, we identify the form of the magnetic couple N_z for the two magnetic material systems under consideration. For permanently magnetic materials, having a remanent magnetization M_r along the axial direction of the film: $(\hat{M}_x, \hat{M}_y) = (M_r, 0)$,

$$N_z = \hat{M}_x \hat{B}_y - \hat{M}_y \hat{B}_x = M_r \hat{B}_y = M_r B_0 \hat{f}(\theta)$$

where θ is the film orientation and B_0 is the amplitude of the applied magnetic field. For a SPM film,

$$N_z = \mu_0 \hat{H}_x \hat{H}_y (\hat{\chi}_x - \hat{\chi}_y) = B_0^2 \hat{h}(\hat{\chi}_x, \hat{\chi}_y, \theta) / \mu_0$$

in which \hat{h} groups the dimensionless dependence of the torque on the susceptibilities $\hat{\chi}_x$, $\hat{\chi}_y$ and the film orientation θ . It is to be noted that the body couple for the SPM film is proportional to the square of the applied field while in the permanently magnetic case, it is linearly proportional.

4. RESULTS

4.1 Asymmetric motion

In this section we discuss several actuator configurations which show asymmetric motion. In all the configurations the applied magnetic field is uniform in space, but its magnitude and direction are varied in time. By tuning the applied field, the initial geometry of the film and its magnetic nature (permanently

magnetic or super-paramagnetic), we have identified four configurations that mimic ciliary motion. For the results presented, the thickness of the film is taken to be $2\mu\text{m}$ and the elastic modulus to be 1 MPa . The drag coefficients are calibrated against computational fluid dynamic (CFD) simulations, details of which will be discussed in section 4.2.1. The results of the simulations are shown in Figs. 1-7.

4.1.1 Partly magnetic film with cracks

The natural cilium is found to have a varying stiffness in the effective and recovery stroke [6]. To use this concept we need to have the film to possess a large bending stiffness in the effective stroke while pushing the fluid and to possess a low stiffness during the recovery stroke. This can be achieved by introducing cracks on one side of the film, while only a part of the film is magnetic. The film is straight initially, is attached at the left end and has cracks of size $0.75\mu\text{m}$ at the bottom. Only 20 % of the film, the end near to the fixed part, is magnetic. The assumed remanent magnetization is 15 kA/m , with the magnetization vector pointing from the fixed end to the free end. The drag coefficients used are $C_x = 30\text{ Ns/m}^3$ and $C_y = 60\text{ Ns/m}^3$. The applied magnetic field is increased linearly to 145 mT in the y direction in 0.6 ms , then rotated by 90° in the next 1.2 ms and finally reduced to zero in the next 0.2 ms . These system properties lead to a magneto-elastic number of 65.25 , a fluid number of 5 and an inertia number of 0.148 . The movement of the film under the action of the applied magnetic field is shown in Fig. 1. When the external magnetic field is applied, the magnetic couples act on the magnetized portion of the film in a counter-clockwise manner, thus rotating the film about the fixed end. Now the drag forces are acting on the top part of the film, which close the cracks, making the film stiff. When the applied field is switched off (Fig. 1(e)), the film will recover elastically and the drag forces act on the bottom part of the film which open the cracks making the film compliant. Such an interaction of magnetic couples, elastic forces and drag forces results in an asymmetric motion, as is clear from Fig. 1.

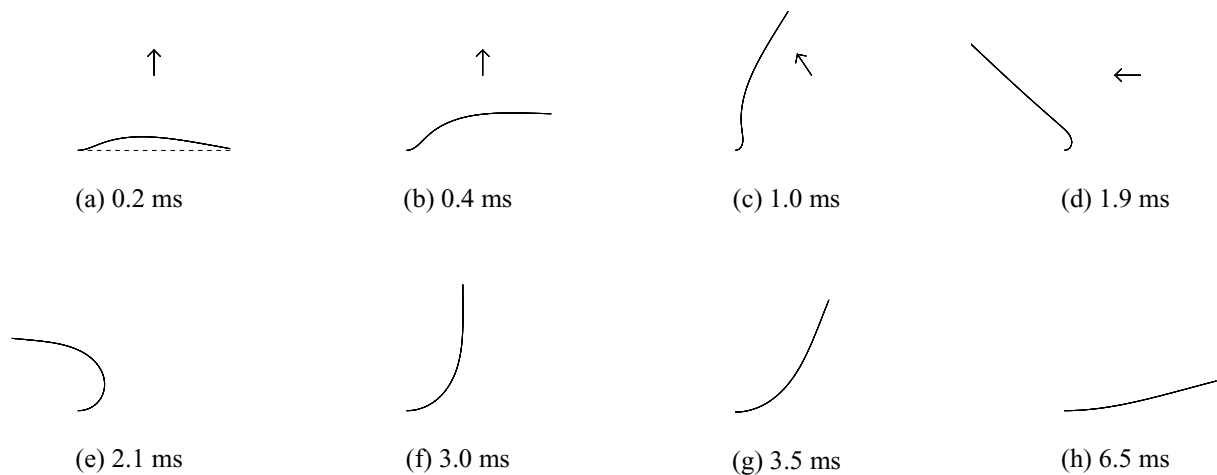


Figure 1: Film with cracks with only a part (20 %) magnetized. The dashed line shows the initial position of the film. The arrow shows the direction of the applied field.

4.1.2 Buckling of a straight magnetic film

A straight horizontal magnetic film with a slight perturbation is used to get the desired asymmetric motion. The film is assumed to have a uniform magnetization with the magnetization vector pointing along the film length, from the fixed end at the left to the free end at the right. The remanent magnetization of the film is taken to be 15 kA/m . The length of the film is $100\mu\text{m}$. The drag coefficients used are $C_x = 30\text{ Ns/m}^3$ and $C_y = 60\text{ Ns/m}^3$. The external field is applied as follows: A field of 30 mT is applied in the negative x direction from $t = 0$ to $t = 1\text{ ms}$ and the field is reduced to zero in the next 0.2 ms . These system properties lead to a magneto-elastic number of 1.125 , a fluid number of 9 and an inertia number of 0.48 . Initially, the magnetization and the applied field are parallel, but with opposite sign, so that the magnetic couple is zero. However, with any perturbation of the film, the equilibrium state becomes unstable and the film will buckle away from the straight configuration. By assuming a uniform magnetization in the film and neglecting drag

forces, the critical field can be calculated. When it buckles the film tries to curl such that the magnetization in the film is aligned with the applied field (Fig. 2(a) – 2(d)). When the applied field is removed, the film returns back to its initial position by elastic recovery. For this configuration, the effective fluid propulsion will take place when the film recovers elastically. Whether the film will buckle up or down depends critically on the sign of the initial imperfection.

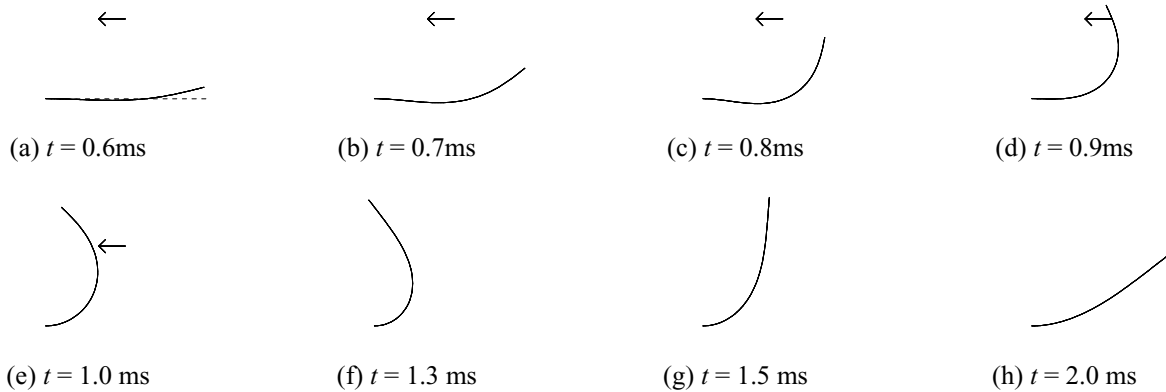


Figure 2: Movement of a perturbed film with the applied magnetic field in opposite direction to the magnetization of the film. The dashed line shows the initial position of the film. The arrow shows the direction of the applied field.

4.1.3 A curled magnetic film

A curled film with remanent magnetization is subjected to a uniform magnetic field. The initial geometry of the film is shown in Fig. 3. The left edge is the clamped end. The direction of the magnetization is along the film with the magnetization vector pointing from the clamped end to the free end. The remanent magnetization of the film is taken to be 15kA/m. An external field of magnitude 9mT is applied at 225° to the x axis from $t=0$ to $t=1$ ms and then linearly reduced to zero in the next 0.2ms. The drag coefficients used are $C_x = 5 \text{Ns/m}^3$ and $C_y = 60 \text{Ns/m}^3$. The radius of curvature of the film is 100 μm . These system properties lead to a magneto-elastic number of 10, a fluid number of 54.68 and an inertia number of 2.91. The physical mechanism of asymmetry is akin to the previous case, except that the film is made to buckle in a predetermined way by a curled geometry, which turns out to exhibit a large asymmetry in motion. The propulsive action in the effective stroke takes place during elastic recovery. In the portion near the fixed end, the magnetic couple acts in a clockwise sense and in the portion near the free end, in a counter-clockwise sense. As a result, these couples tend to bend the film, such that the curvature of the film

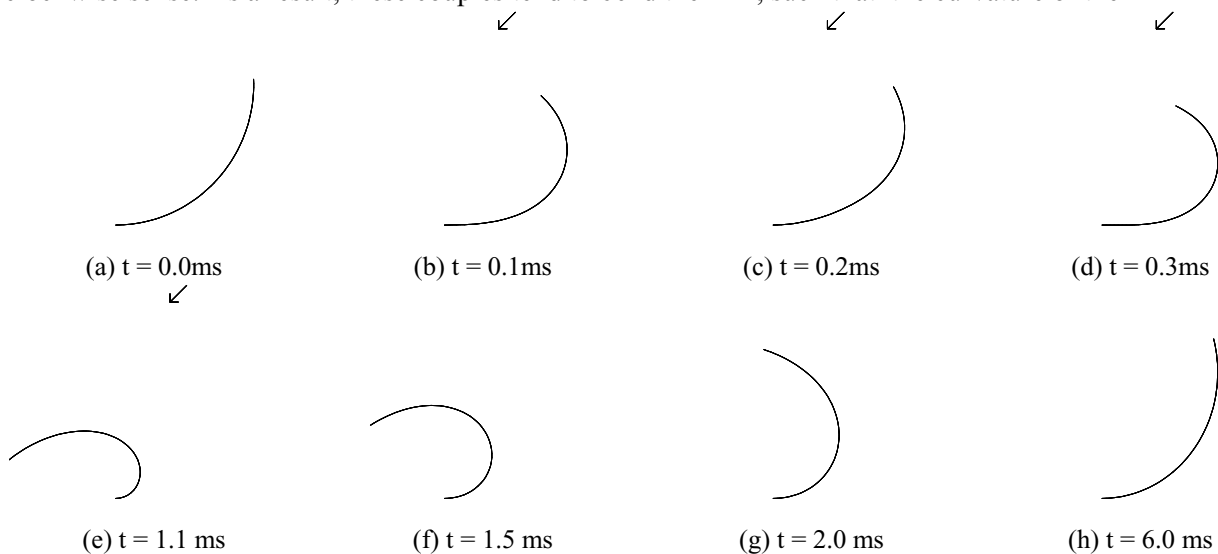


Figure 3: Movement of a permanently magnetic film. The arrow shows the direction of applied field.

increases, bringing the ends of the film closer together (this behavior is similar to that of a natural cilium). Here, the asymmetry is larger than the previous case as can be observed from Figs. 2 and 3.

4.1.4 Super-paramagnetic film

A super-paramagnetic film which is anisotropic in its magnetic susceptibility and which is tapered along its length is subjected to a rotating magnetic field. The assumed susceptibilities are 4.6 and 0.8 in the tangential and normal directions, respectively. The thickness of the film varies linearly along its length, being $2\mu\text{m}$ at the left (attached) end and decreasing to $1\mu\text{m}$ at the right end. A magnetic field of 31.5mT is rotated from 0° to 180° in $t=10\text{ms}$ and then kept constant for the rest of the time. The drag coefficients used are $C_x = 30\text{Ns/m}^3$ and $C_y = 60\text{Ns/m}^3$. These system properties lead to a magneto-elastic number of 23.6, a fluid number of 0.9 and an inertia number of 4.8×10^{-3} . When a rotating field is applied, the free end portion of the beam is rotated through 135° and a U bend is formed near the fixed end (Fig. 4(e) and 4(f)). It is to be noted that the portion of the beam near the free end is nearly straight. This is because the magnetization of the film in this region is almost aligned to the applied field (which is evident from the magnetization vectors shown on the film in Fig. 4). As a result, the normal component of the field is low, and hence the moment is less as well. In this situation it is in the part of the film near the U bend, where the magnetic couple distribution (which tends the film to bend) balances the elastic forces (which tends the film to become straight again), hence "freezing-in" the bent shape. When compared with other parts of the beam, at the U bend portion of film the magnetic couples are large. On the portion of the film between the free end and the U bend, anticlockwise moments are acting. On the portion between the fixed end and the U bend, clockwise moments are acting (Figs. 4(e), 4(f) and 4(g)). Due to the tapered nature of the film, the clockwise moments are larger than the anticlockwise moments. Under the influence of such a system of moments, the film becomes more curved, the end to end distance decreases and the film recovers. As the beam recovers elastically the U bend propagates to the free end of the beam. It is to be noted that the film recovers in the presence of magnetic forces, i.e. the recovery is not an elastic one, but controlled by magnetic forces, keeping the film low. This phenomenon can be exploited to provide a large asymmetry in motion of the film during the forward and return stroke. A larger field will result in larger curvature of the U bend, forcing the film to stay lower, enhancing the efficiency of the return stroke.

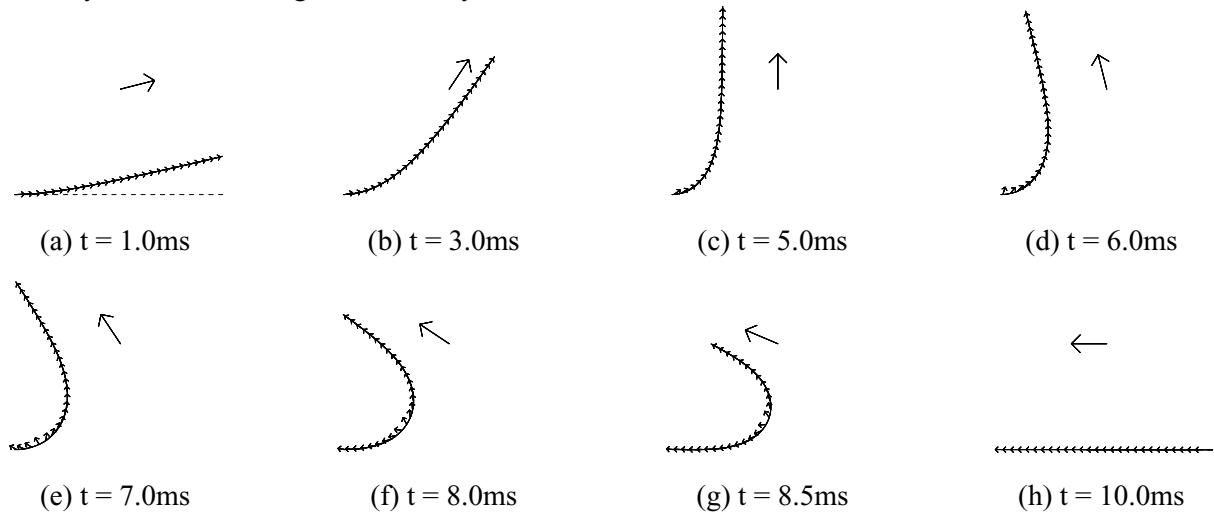


Figure 4: Super-paramagnetic film in a rotating magnetic field. The big arrow shows the direction of the applied magnetic field. The small arrows show the magnetization.

4.2 Fluid propulsion

In the magneto-mechanical model, the presence of the fluid is incorporated through drag relations that account for the surface tractions as a function of the velocity. The specific values for the drag coefficients used in the previous section have been calibrated through a comparison with a fully-coupled solid-fluid model. This model and the calibration procedure will be discussed in this section. Moreover, we will also investigate how efficient the four asymmetric motions are in actually propelling fluid. We will demonstrate that the swept area by the film tip is one-to-one related to the fluid propelled. The Lagrangian solid dynamics model used to study the magneto-mechanical behavior of the films (section 2) is explicitly coupled to an

Eulerian fluid dynamics code based on the method used in [5]. Fluid inertia is neglected, so the fluid model effectively solves the Stokes equations. The explicit coupling between the two domains is established through Lagrange multipliers. Input to the fluid dynamics model are the positions and velocities of the film at all times which result in a full velocity field in the fluid. We calculate the drag forces on the film as tractions via the stress tensor in the fluid. The traction distribution is subsequently imposed as surface tractions in the solid dynamics model through Eqn. 6.

4.2.1 Calibration of drag coefficients

To calibrate the drag coefficients, coupled solid-fluid simulations are performed using a periodic arrangement of cilia in a micro-fluidic channel. The dimensions of the unit-cell analyzed are 400 μm in width (horizontal) and 500 μm in height. No-slip boundary conditions are applied at the top and bottom boundaries of the channel and periodic boundary conditions at the left and right ends of the unit-cell. The viscosity of the fluid is taken to be that of water (1×10^{-3} Pas). The film is placed at the center of the channel to avoid any interaction with the boundary. From the coupled solid-fluid simulations we get the trajectory of the free end. We then perform simulations using the magneto-mechanical model (section 2) with the assumption that the fluid exerts tractions that are proportional to the velocity, on the film as mentioned in section 2.1. We vary the drag coefficients to match the trajectory of the free end obtained from the coupled solid-fluid simulations. The results are depicted in Fig. 5, clearly showing that the agreement between the uncoupled and fluid-coupled trajectories is very good. The drag coefficients obtained here have been used for the simulations presented in section 4.1.

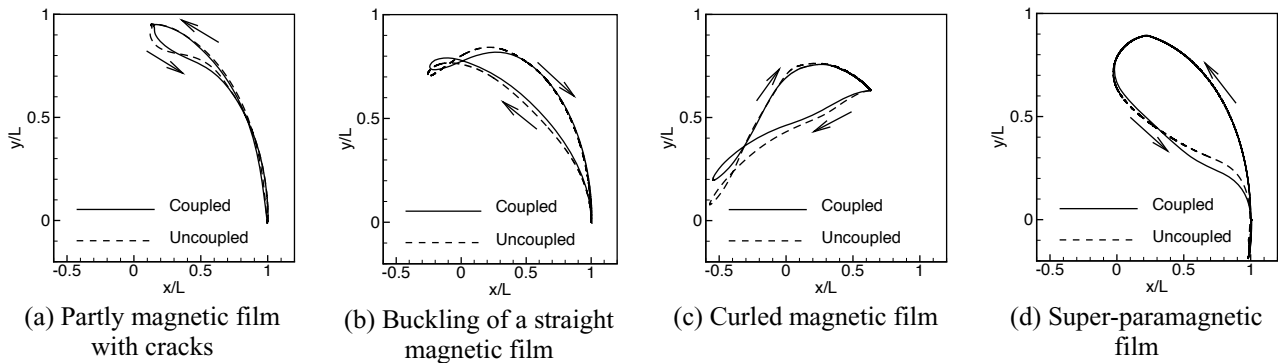


Figure 5: Trajectory of the free end for various cases obtained when calibrating the drag coefficients used in the uncoupled solid-drag simulations of Section 4.1 with the fully coupled solid-fluid simulations. For the magnetic film with cracks, the crack length is taken to be 0.1 μm ; the parameters of the three other configurations coincide with section 4.1. The arrows indicate the direction of motion of the trajectory.

4.2.2 On using the area swept by the free end as a measure of effectiveness

At low Reynolds numbers, asymmetric motion is required to propel the fluid. To study how much fluid is propelled for a given asymmetric motion, we studied two configurations: the curled permanently magnetic film (Fig. 3) and the SPM film (Fig. 4). As a measure for the asymmetry, we compute the area swept by the

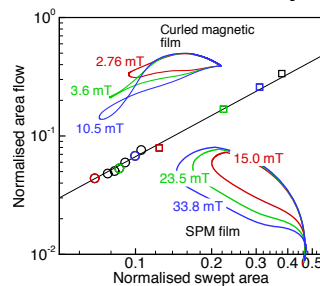


Figure 6: Relation between swept area and fluid propelled. Square and circle represent SPM film and curled magnetic films, respectively. Trajectories shown at the top and bottom belong to curled magnetic and SPM film, respectively, obtained by changing the magnetic field. The color of the symbols correspond to the respective color of the trajectory. The areas are normalized with the maximum area that can be swept (maximum area that can be swept is $\pi L^2 / 2$).

free end of the film. To vary this area we vary the magnitude of the magnetic field applied and perform coupled solid-fluid simulations. The corresponding swept area and the total flow across the channel in one cycle is computed. The domain for which the calculations are performed, is the same as that used for the calibration of the drag coefficients, discussed above. The dependence of fluid propelled (the area flow per cycle) on the swept area is shown, for both the cases, in Fig. 6. The fluid propelled is seen to vary linearly with the swept area. This suggests that the swept area can be used as a measure of effectiveness of the cilium, representing the fluid volume displaced. In the following Section, we will use this to investigate the efficiency of fluid propulsion as a function of the system parameters.

5. EFFICIENCY SURVEY AND DISCUSSION

A parametric study of the curled magnetic film and the super-paramagnetic film is performed next. The parameters that govern the response of the actuator system are the inertia number, the fluid number and the magneto-elastic number. The performance of the system is quantified in terms of the swept area (as a measure of the asymmetry and associated fluid flow) and the time taken by the film to reach its initial position. The actuator system based on its material properties, its geometry and the fluid to be propelled can have different fluid and inertia numbers. Fixing them establishes the system. Different set of these numbers

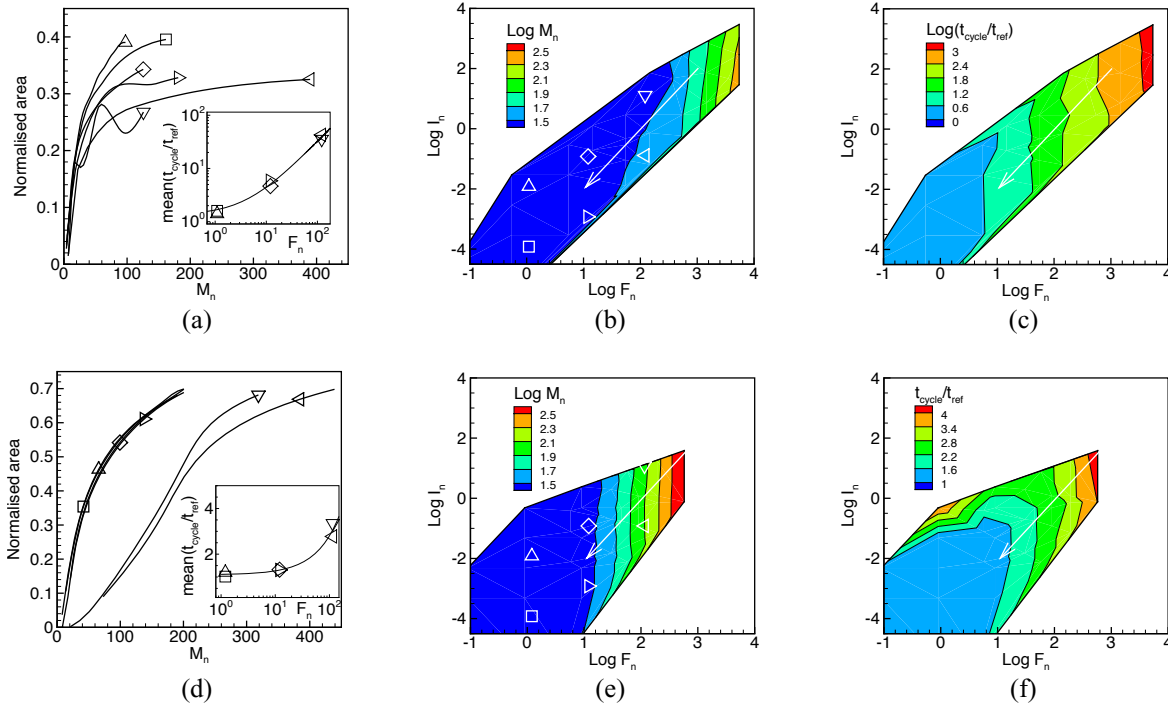


Figure 7: Efficiency study of curled magnetic film ((a), (b) and (c)) and SPM film ((d), (e) and (f)). (a) and (d) show the evolution of the area swept by the films as M_n is varied. The inserts in (a) and (d) show the mean time in which the films complete one cycle. The symbols represent systems with different I_n and F_n , which can be found from (b) and (e). M_n needed to sweep a normalized area of 0.2 is shown in (b) and (e). While sweeping this area the respective time taken by the film to complete one cycle is shown in (c) and (f).

refer to different systems. For a set of these systems the magneto-elastic number is varied and the swept area and the time to reach the initial position is noted. The ingredients in the dimensionless parameters are as follows: L is taken to be the length of the film, h is the thickness of the film, the length is varied from 100 to 1000 μm and the aspect ratio L/h is varied from 10 to 200. The density ρ of the film is varied from 600 to 8000 kg/m^3 , the drag coefficient C_x is varied from 6 to 600 Ns/m^3 , while the ratio C_y/C_x is kept the same, and the time scale t_{ref} is taken to be the time in which the load is applied. For a magnetic film it is the time during which the magnetic field is applied and for the SPM it is the time during which the magnetic field is rotated.

The area swept by the free end of the film for different systems (varying inertia number and fluid number) by varying the magneto-elastic number is shown in Figs. 7(a) and 7(d), for the magnetic film and SPM film respectively. The area is normalized with the maximum area that can be swept by a given system (maximum area that can be swept is $\pi L^2 / 2$). This plot shows that for a given magneto-elastic number, the swept area decreases with an increase of fluid number. As the fluid number increases, the drag force opposing the motion of the film increases, hence the deformation of the film is less, thus sweeping less area. The inserts in Fig. 7(a) and 7(d) represent the mean time taken by the film to complete one cycle. It can be seen that this time scales linearly with F_n , representative of the relaxation time of a spring-damper system.

The magnetic number needed to sweep a normalized area of 0.2 for different systems is shown in Figs. 7(b) and 7(e). As the fluid number increases, we need a large magneto-elastic number to sweep a given area, for a given inertia number. When the fluid number is kept constant, we need slightly lower magneto-elastic number to sweep the same area at large inertia numbers. This is because larger inertia number leads to low elastic forces resisting the film motion. This dependency of the swept area of the film is large at small fluid numbers when compared to high fluid numbers. This is due to the fact that the viscous forces dominate over the inertial forces at high fluid numbers. The arrow points in the direction of reducing the size of the film while, keeping the aspect ratio constant. It can be seen that, as the size of the film decreases, the film enters a region of low F_n and low I_n , where the film's motion is insensitive to a change in F_n and I_n . When sweeping an area of Fig. 7(b) and 7(e), the time taken by different systems to return to their initial position is shown in Figs. 7(c) and 7(f), respectively. It can be seen for the magnetic film that it takes longer for the film to return to its initial position when the fluid number is increased and is independent of the inertia number. But in the case of SPM film, because of the whip-like return stroke, some dynamic effects are observable at larger inertia numbers, hence these systems take longer time to return to their initial position at large I_n .

6. SUMMARY

We have presented a concept for microfluidic manipulation in microchannels based on magnetic films actuated by external fields. The behavior of the film is quantified using dimensionless parameters. We explored different configurations which lead to fluid propulsion in microchannels. It is shown that the fluid propelled scales linearly with the area swept by the tip of the film. Finally, we have quantified the behavior of the film as a function of those dimensionless parameters.

ACKNOWLEDGEMENTS

This work is a part of the 6th Framework European project 'Artic', under contract STRP 033274.

REFERENCES

- [1] den Toodner, J., *et. al.* (2008). Artificial cilia for active micro-fluidic mixing, *Lab Chip*, **8**, 533-541.
- [2] Khatavkar, V., *et. al.* (2007). Active micromixer based on artificial cilia, *Phys. Fluids*, **19**, 83605.
- [3] Evans, B. A., *et. al.* (2007). Magnetically actuated nanorod Arrays as biomimetic Cilia, *Nano Lett.*, **7** (5), 1428 -1434.
- [4] Malvern, L. E. (1974). *An Introduction to the mechanics of continuous media*. John Wiley & sons.
- [5] Jackson, J. D. (1974). *Classical Electrodynamics*. John Wiley & sons.
- [6] Gray, J. (1922). The mechanism of ciliary movement. *Proc. R. Soc.* **93**, 104-121.